Systematic motion of magnetic domain walls in notched nanowires under ultrashort current pulses

A. Pivano and V. O. Dolocan[*]

Aix-Marseille Université, CNRS, IM2NP UMR7334, F-13397 Marseille Cedex 20, France
(Received 20 June 2017; revised manuscript received 8 November 2017; published 27 December 2017)

The precise manipulation of transverse magnetic domain walls in finite/infinite nanowires with artificial defects under the influence of very short spin-polarized current pulses is investigated. We show that for a classical $3d$ ferromagnet material like nickel, the exact positioning of the domain walls at room temperature is possible only for pulses with very short rise and fall time that move the domain wall reliably to nearest neighboring pinning position. The influence of the shape of the current pulse and of the transient effects on the phase diagram current-pulse length are discussed. We show that large transient effects appear even when $\alpha = \beta$, below a critical value, due to the domain wall distortion caused by the current pulse shape and the presence of the notches. The transient effects can oppose or amplify the spin-transfer torque (STT), depending on the ratio β/α. This enlarges the physical comprehension of the domain wall (DW) motion under STT and opens the route to the DW displacement in both directions with unipolar currents.

I. INTRODUCTION

Current induced magnetic domain wall motion (CIDWM) in nanowires or nanostrips is a highly active research field [1,2] with applications in high-density and ultrafast nonvolatile data-storage devices like the racetrack memory [3] or for logic devices [4]. In the racetrack memory, the data processing is based on the controlled displacement between precise distinct positions of the domain walls (DWs) due to the transfer of angular momentum (spin-transfer torque) from a spin-polarized electric current. To achieve precise positioning of DW, artificial constrictions, or others, patterned geometrical traps are usually used, which create an attractive pinning potential for the DW. Different types of traps were studied in cylindrical or flat/strip nanowires [5–8], along with the possible interaction between the DWs [9,10]. In some cases, depending on the pinning potential, the DW displacement between pinning sites can display a chaotic behavior [11] or a stochastic resonance [12] under harmonic excitation.

The required currents for STT based DW movement are usually high (~ 1 A/μm^2), which limits the applicability due to Joule heating. To displace accurately the DWs between the pinning sites, the current density should be kept at relatively low values and/or very short current pulses should be applied. Experimentally, it was observed that an efficient DW motion is reached for pulses in the nanosecond regime [13] and that the resonant excitation of the DW by a short train of current pulses decreases the depinning current [14]. More recently, the effect of the temporal and spatial shape of the current pulse was highlighted [15–17]. It was shown that a fast changing current with an ultrashort pulse rise time decreases the critical current density due to the dependence of the DW motion on the time derivative of the current [18] and leads to high DW velocity [19]. Another aspect of the CIDWM under short pulses is the existence of important transient effects related with the DW inertialike behavior [13,20–23] due to deformation of the wall. The consequences are a delayed response at the current onset and at the end of the current pulse. The theoretical

and experimental results show that the distance traveled by a DW is almost proportional to the current pulse length and that the transient motion depends on the variation of the generalized angle of the wall, the wall width, and the ratio of the damping (α) and nonadiabatic (β) parameters [20,21]. For very short pulses (one nanosecond), the transient displacement is comparable with the steady-state motion [24]. A DW that propagates without deformation should display no inertia [25] like in cylindrical nanowires [26] or in certain perpendicular magnetic anisotropy systems [27]. The absence of inertia will allow a fast response to external forces while the transient DW displacement after the application of the pulse limits the application in fast devices. In the main time, it was recently demonstrated that inertialike behavior of a DW can be also an advantage when ultrashort optical pulses are used [28] with applications in the optical recording. Moreover, in systems with strong spin-orbit coupling where additional contributions from spin-Hall effect complicate the DW dynamics, a DW tunable inertia was proposed [29]. Before studying more complex systems, the influence of the transient effects on the systematic DW movement under ultrashort spin-polarized current pulses should be completely understood in a classical $3d$ ferromagnet like nickel, which is the aim of this paper.

In this paper, we address the systematic motion of a magnetic transverse DW between fixed artificial constrictions (notches), when submitted to a series of ultrashort spin-polarized current pulses (transient regime) at low and room temperature. The artificial constrictions are situated at regular positions in a flat finite or infinite nanowire with only in-plane (shape) anisotropy like in a classical $3d$ ferromagnet. We determine the influence of the current pulse shape (rise and fall time) on the motion of the DW. We show that, even at zero temperature, there is a transition region between the different bands in the current-pulse time phase diagram, each band corresponding to the positioning of the DW at a well-defined notch. Our results show that, at room temperature, the precise positioning can be achieved only by very short pulses with very short rise and fall times that displace the DW by only one notch at a time. Therefore, to move a DW several notches reliably, a sequence of very short pulses should be used. By examining the influence of the damping and nonadiabatic parameters, we

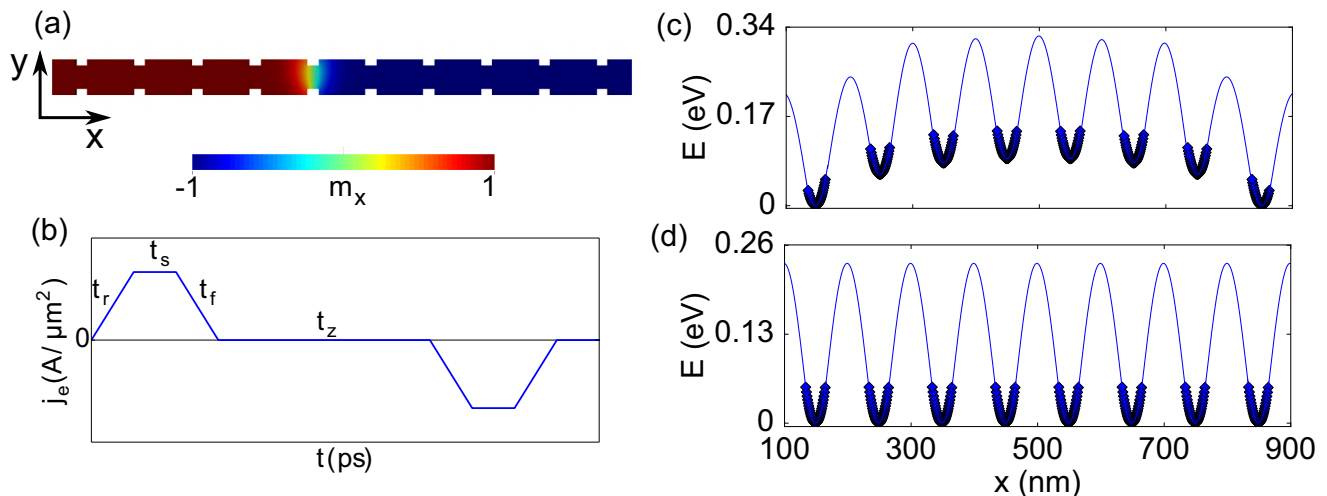_____
[*]voicu.dolocan@im2np.fr

FIG. 1. (a) Simulated structure: planar nanowire with ten symmetric double notches. The equilibrium position of a pinned DW is shown in the finite case. (b) Definition of current pulse with its temporal characteristics. Two successive current pulses with opposite polarity are shown. The normalized potential pinning energy for finite and infinite cases as determined by micromagnetic simulations (symbols) are shown in (c) and (d), respectively. The line is a fit as described in the text.

show that when $\beta = 0$ the transient effects (automotion) of the DW are very large and oppose the STT, being observed in the phase diagrams as predicted [20]. The transient effects are related with the change in the DW structure that is due to a combination of factors: pinning potential of the notches which induces a sufficient variation of the DW angle [30], position of the DW inside the potential well (different restoring force), low damping parameter, and shape of the current pulse. Contrary to expectations, the transient effects also appear when $\alpha = \beta$, below a critical value. For $\beta > \alpha$, the transient effects can oppose or amplify the STT, thus explaining the oscillatory DW depinning at higher currents observed experimentally [13]. This brings new physical insight into CIDWM under STT and paves the way for systematically displacing DW in nanowires in both directions using only unipolar current pulses.

This article is organized as follows. In Sec. II, we present the micromagnetic and the stochastic 1D model used to calculate the pulsed DW dynamics. In Sec. III, we compute and investigate the phase diagram of the DW dynamics for a finite and infinite nanostrip at $T = 0$ K and room temperature. Discussion and concluding remarks are presented in Sec. IV.

II. MODEL

We study numerically the systematic motion of a pinned transverse domain wall in a finite or infinite Ni nanostrip with symmetric rectangular notches. The finite strip has a length $L_x = 1$ μm, a cross section of $L_y \times L_z = 60 \times 5$ nm^2, and has ten rectangular symmetric double notches separated by 80 nm. The results presented below are for notch dimensions of $20 \times 9 \times 5$ nm^3. The variation of length and depth of the notches does not influence much the physics of phase diagrams presented in Sec. III. The notch depth influences the depinning current as the potential barrier increases, while the notch length influences lightly the depinning current and mostly the slope of the potential wells.

Figure 1(a) shows the equilibrium position of a head-to-head transverse DW in the notched nanostrip using the parameters of nickel: saturation magnetization $M_s = 477$ kA/m, exchange stiffness parameter $A = 1.05 \times 10^{-11}$ J/m, spin polarization $P = 0.7$, and damping parameter $\alpha = 0.05$. The DW is moved by a series of spin polarized current pulses applied along the x axis. The geometry of the current pulse is described in Fig. 1(b), with t_r, t_s, t_f, and t_z the rise, stable, fall time, and zero-current time, respectively. The nonadiabatic parameter is set to $\beta = 2\alpha$, if not specified otherwise.

The DW dynamics was computed using 3D micromagnetic simulations with the MUMAX3 package [31] and with the one-dimensional DW model [32,33]. In both cases, the magnetization dynamics is determined from the Landau-Lifschitz-Gilbert (LLG) equation with adiabatic and nonadiabatic spin-transfer torques [34]:

$$\dot{\mathbf{M}} = -\gamma_0 \mathbf{M} \times \mathbf{H}_{\text{eff}} + \alpha(\mathbf{M} \times \dot{\mathbf{M}}) - (\mathbf{u} \cdot \nabla)\mathbf{M} + \beta\mathbf{M} \times (\mathbf{u} \cdot \nabla)\mathbf{M}, \tag{1}$$

where γ_0 is the gyromagnetic ratio, $\mathbf{u} = \mathbf{j}_e P \mu_B / e M_s$ is the spin drift velocity, P the spin polarization of conductions electrons, μ_B the Bohr magneton, and $\mathbf{j}_e$ the applied current density. No additional exotic torques (like the ones due to the spin-Hall or Rashba effect) were considered.

For the micromagnetic computations, the strip was discretized into a mesh with a cell size of $2 \times 3 \times 2.5$ nm^3, inferior to the exchange length ($\sim$5 nm). The DW dynamics in a finite wire is compared with the one of an infinity long wire where the magnetic charges at the ends of the nanostrip are compensated. The average position of the DW center (X) is extracted for each simulation (in the axial x direction) along with the azimuthal angle (ψ) of magnetization in the yz plane. No magnetocrystalline anisotropy is considered; the shape anisotropy insures that the easy axis is in-plane. The effect of the temperature is studied both micromagnetically and with the 1D model. The 1D model of the DW (collective coordinates X and ψ) supposes that the DW is rigid and gives a

quasiquantitative understanding of the motion of the DW. The Langevin equations of motion of the DW [2,35] are detailed in the Supplemental Material [36].

The pinning potential energy is determined from quasistatic micromagnetic simulations and is shown in Figs. 1(c) and 1(d) for the finite case and the infinite case, respectively. The pinning potential determined by fitting the micromagnetic results is harmonic inside the notches and sinusoidal between them:

$$V_p(x)$$
$$= \begin{cases} \frac{1}{2} k_i (x + x_i)^2, & \text{for } x_i - L \leqslant x \leqslant x_i + L, \\ V_0 \cos(2\pi f x + \phi_{i,i+1}), & \text{for } x_i + L < x \leqslant x_{i+1} - L, \end{cases}$$
$$(2)$$

with k_i the stiffness constant and x_i the DW stable equilibrium position of the site i, and $\phi_{i,i+1}$ the phase between the i site and its nearest neighbor. V_0 and f correspond respectively to the effective height of the potential and its spatial frequency. For the finite case, the stiffness constant varies from 7.07×10^{-5} N/m to 6.77×10^{-5} N/m, when moving from the center of the nanowire to its ends. In the infinite case, the stiffness constant is equal to 7.16×10^{-5} N/m for all the pinning sites and $L = 16.5$ nm. The expression [Eq. (2)] was used in the equations of the 1D model through the pinning field H_p included in H_{eff}.

The pinning energy is controlled by the dimensions and distance between the notches. A clear difference is observed between the two potentials due to edge dipolar energy. In the finite strip, the depinning field decreases from 39 Oe, in the central wells, to 26 Oe when the DW is closed to the two ends of the strip. This is due to the attractive interaction between the DW and magnetic surface charges located at the sides [37]. As a result, the potential wells are asymmetric in energy along the strip and their energy minima decrease when the distance between the notches and the ends of the strip is reduced. In contrast, for the infinite case, each well has the same depinning field and energy barriers.

III. RESULTS

Our analysis of the DW dynamics begins with the study of the differences between a finite and an infinite nanostrip at $T = 0$ K. Afterwards, the influence of the pulse shape is discussed and the particularities of the DW motion at room temperature. The last subsection details the results when the damping and nonadiabatic parameters are varied and their influence on the transient displacement.

A. Phase diagrams at $T = 0$ K

To characterize the systematic motion of the DW between the notches, we computed point-by-point phase diagrams for all systems with the 1D DW model for a large range of pulse duration and current amplitude. We compare our 1D results with phase diagrams computed micromagnetically on less points than the 1D calculus. A similar micromagnetic computation will require an enormous execution time. The control parameters are the amplitude, the duration, and the shape of the current pulses. The range of the current amplitude ($\leqslant 10$ A/μm^2) is chosen to have only viscous motion (no
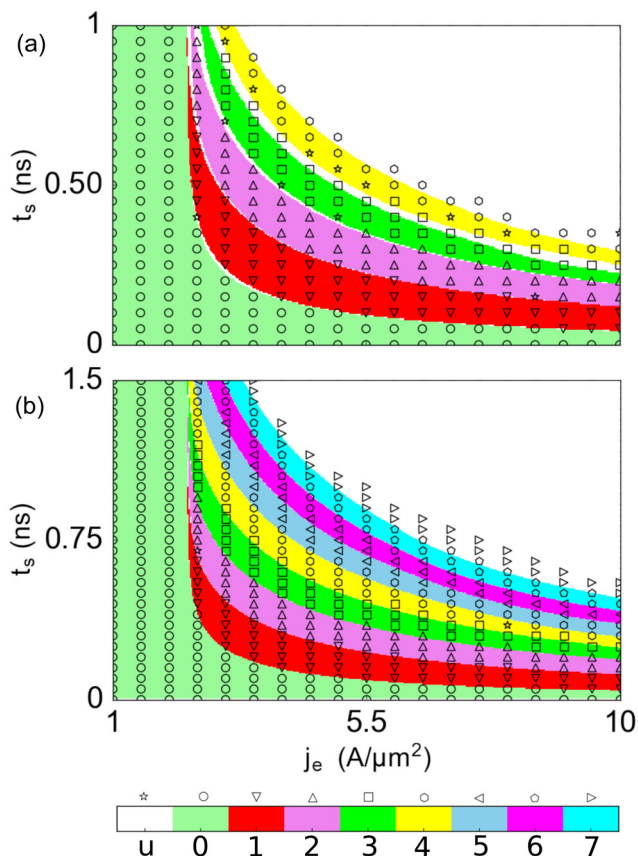

FIG. 2. Phase diagram for a DW at $T = 0$ K in a finite (a) and infinite (b) nanostrip in the parameter space stable-time–current amplitude with $t_r = t_f = 5$ ps and $t_z = 10$ ns. The total time of the periodic pulses is 350 ns. The micromagnetic results (scattered symbols) are compared to the 1D model (colored regions). The diagrams show only a few bands due to the finite size of the wire or due to the number of notches used. The upper right region is due to the finite size of the nanowire or of the simulated window (infinite case).

precession) for the pulse duration used ($\lesssim 1.5$ ns). The pulse duration range is selected to be on the same order of magnitude with access or reading/writing time in possible magnetic memories based on DW.

The phase diagram, in the parameter space stable time–current amplitude, which characterizes the DW dynamics in the finite nanostrip at $T = 0$ K, is shown in Fig. 2(a). The diagram represents 200×400 point-by-point integration with a fourth order Runge-Kutta scheme. The micromagnetic results (scattered symbols) are compared with the 1D results (colored regions). The DW is initialized in the left central well and a series of periodic bipolar current pulses are applied during 350 ns to move periodically forth and back the DW between two desired notches. The pulse characteristics are $t_r = t_f = 5$ ps and $t_z = 10$ ns. The influence of t_r and t_f is discussed below. The value of t_z (10 ns) was chosen to correspond to the return to equilibrium time of the DW at room temperature. The t_z can be reduced to 3 ns for $T = 0$ K, without a change of the phase diagrams. In Fig. 2(a), several regions are visible, each region corresponding to one state of the DW oscillation. The first state which appears is the

pinned state, noted state zero in the micromagnetic simulation, and corresponds to the DW being pinned in the initial notch. After the pulse ends, the DW behaves like a damped harmonic oscillator. The state zero is observed for all t_s, when the external current j_e is inferior to the depinning current 2.31 A/μm^2. This state is also observed at higher currents (until 10 A/μm^2), when the stable time t_s is low (between 0 ps and 55 ps). The diagram displays other bands, where the DW oscillates periodically between the same two potential wells, which can be next neighbors (noted as band 1) or not, until the fifth state that corresponds to the periodic oscillation between the initial notch and the fourth notch to the right (band 4) hopping the three notches in between. The number of bands is given by the considered finite size of the nanostrip. The second state (next-neighbors notches noted band 1) is observed up to $t_s = 0.96$ ns at $j_e = 2.3308$ A/μm^2, while the other bands continue above $t_s = 1$ ns. Thus the DW can cross several notches back and forth for a given current pulse characteristic. We observe that the interband transitions are characterized by an unintended state (state u), where the DW oscillation does not take place between the desired positions. This transition is more pronounced between the last two bands. The micromagnetic results, which are superimposed on the 1D results, give quantitatively the same results until the fourth state, after which a small shift appears in the t_s and j_e values, but the bands are qualitatively the same. The upper right region, which corresponds to an unwanted state, is due to the finite size of the nanowire; here the DW is pinned at the nanowire end.

In the infinite case, the DW is initialized in the first well from the left. A phase diagram similar to the finite case is shown in Fig. 2(b). This diagram contains three more bands than the finite case, which correspond to additional states where the DW oscillates between two notches, starting from the initial one, separated by four intermediate notches (band 5) until six intermediate notches (band 7). To have a better visibility over these new bands we computed the DW dynamics for t_s up to 1.5 ns on 300 $\times$ 400 points. We observe that the bands 1 and 2 exist until $t_s = 1.045$ ns and $t_s = 1.27$ ns, respectively, at $j_e = 2.3308$ A/μm^2, while the other bands continue above 1.5 ns. The interband transition (band u) is observed between the bands zero and one around $j_e = 3$ A/μm^2 and $t_s = 250$ ps. For the superior bands, the interband transition at boundaries is quasi-nonexistent, which shows that the infinite case is more stable than the finite case. In both cases, the 1D model gives quantitatively the same results as the micromagnetic simulations in the three first bands and quasiquantitatively in the others (a shift in values is visible). As for the finite case, the upper right region appears due to the finiteness of the simulated length of the nanowire, even if the end charges are suppressed. If a longer simulated window is considered, other superior bands will follow as seen for example in Fig. 5 or Fig. 6.

The influence of the pulse shape is detailed in Fig. 3 for the infinite wire as calculated with the 1D model. In panel (a), the pulse shape is symmetric as $t_r = t_f = 5$ ps and $t_z = 10$ ns, while in panels (b) and (c) the pulse shape is asymmetric, $t_r \neq t_f$, with t_z is kept constant at 10 ns. The values of t_r and t_f were varied between 5 ps and 300 ps. In panel (b), the case with $t_r = 5$ ps and $t_f = 300$ ps is shown, while in panel (c),
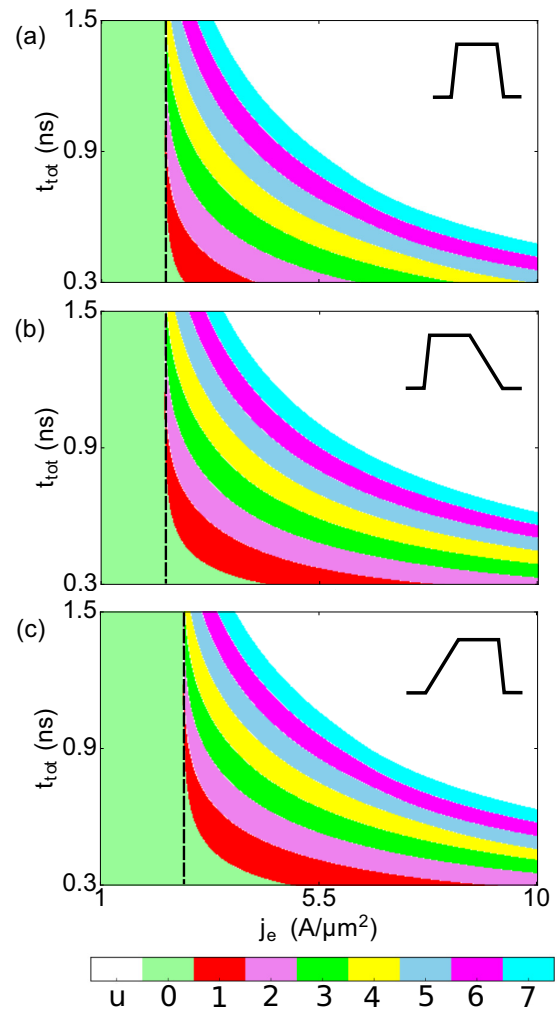

FIG. 3. Influence of the pulse shape on the phase diagram for a DW at $T = 0$ K in an infinite nanostrip. The parameter space is the total time $(t_r + t_s + t_f)$ vs current amplitude. (a) Symmetric pulse with $t_r = t_f = 5$ ps and $t_z = 10$ ns; asymmetric pulse with (b) $t_r = 5$ ps, $t_f = 300$ ps, and $t_z = 10$ ns and (c) $t_r = 300$ ps, $t_f = 5$ ps, and $t_z = 10$ ns. The upper right region is due to the finite size of the simulated window.

the one with $t_r = 300$ ps and $t_f = 5$ ps. In the three panels, the total time ($t_{tot} = t_r + t_s + t_f$) is shown starting from 300 ps, to be able to compare the diagrams evolution with the pulse shape. We observe that the first depinning current depends mainly on the rise time as depicted in panels (a) and (b), where only the fall time is varied. In these cases, the first depinning current is the same and equal to 2.31 A/μm^2. The influence of the t_f is an offset of the bands along the total time axis; therefore, if t_f is decreased the second band is shifted to shorter times and almost disappears from the shown phase diagram. The influence of the rise time manifests itself also as an offset of the bands to larger times, but also to larger currents and therefore a higher first depinning current equal to 2.69 A/μm^2. The first depinning current for a total time of 0.3 ns is 2.78 A/μm^2 for the symmetric pulse, rising to 4.54 A/μm^2 [panel (b)] and 5.03 A/μm^2 [panel (c)] in the asymmetric case. The micromagnetic calculation (not shown)
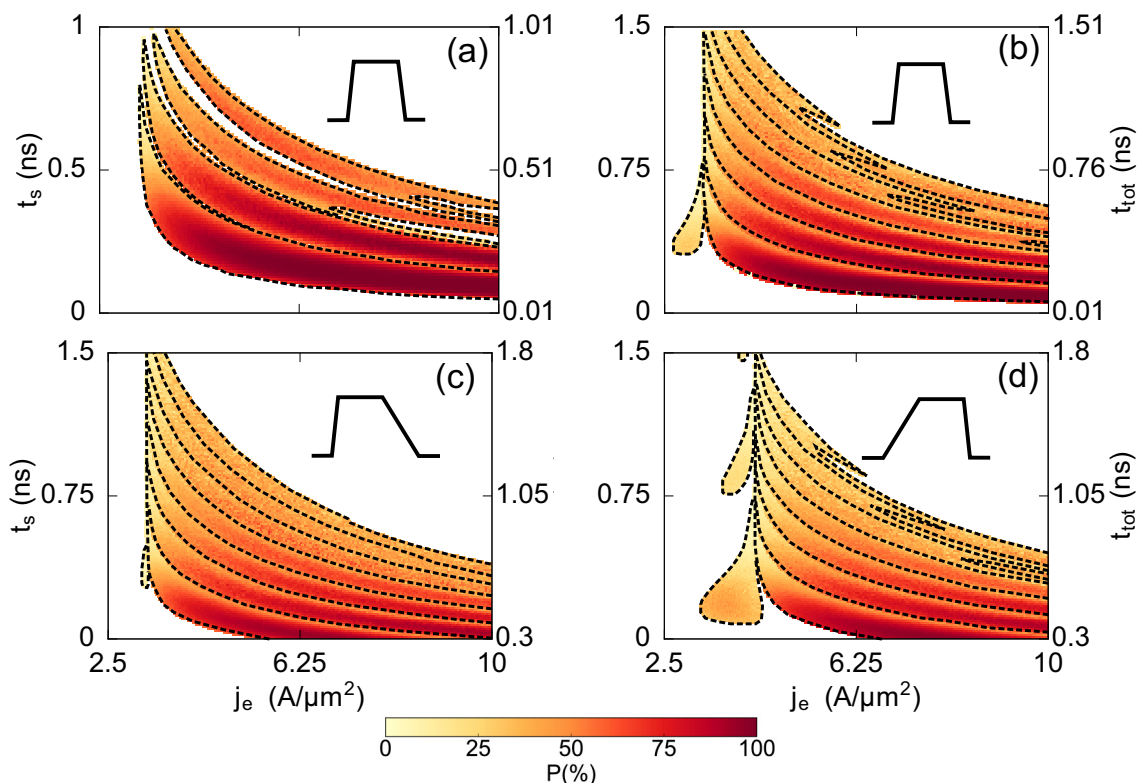
FIG. 4. Probability of DW motion in different bands for the finite strip (a) and the infinite strip (b)–(d) at $T = 293$ K. (a), (b) A symmetric pulse is applied with the characteristics $t_r = t_f = 5$ ps, after an initial and final t_z of 10 ns. (c) An asymmetric pulse is applied with pulse shape $t_r = 5$ ps, $t_f = 300$ ps, after an initial and final t_z of 10 ns. (d) An asymmetric pulse is applied with pulse shape $t_r = 300$ ps, $t_f = 5$ ps, after an initial and final t_z of 10 ns. The damping parameter is taken as $\alpha = 0.02$ and $\beta = 2\alpha$. The band pockets, which appear in the panels (b) to (d) on the left, correspond to the band -1. The dotted lines are guide to the eyes and represent the band's edges.

gives similar results as the ones shown in Fig. 2, meaning a small offset of the bands compared with the ones calculated with the 1D model starting from the fourth band.

The dependence of the depinning current on the rise time was deduced from the linearized equation of motion in the 1D approximation, as the force on the DW can be written as [15,18]

$$\ddot{X} = -\frac{\dot{X}}{\tau_d} - \frac{1}{m}\frac{dE}{dX} + \frac{\beta}{\alpha\tau_d}u + \frac{1+\alpha\beta}{1+\alpha^2}\dot{u}, \qquad (3)$$

where $m = \frac{2\alpha S\mu_0 M_s \tau_d}{\Delta\gamma_0}$ is the DW mass, $\tau_d = \frac{1+\alpha^2}{\alpha\gamma_0 H_k}$ is the damping time, with H_k the anisotropy field, Δ is the DW width, and E is the pinning energy. The force on the wall depends on the current and its derivative; therefore, a shorter rise time increases the derivative term which leads to a decreasing of the depinning current and vice versa. For the present results, the damping time is 0.27 ns (0.68 ns for $\alpha = 0.02$); therefore, the DW is in the transient regime for the pulse duration used.

B. Temperature dependence

The temperature influences the systematic motion of the DW by modifying the DW relaxation in a potential well after an applied current pulse. The oscillations during the DW relaxation could be sustained by the thermal noise, which could lead to a jump to the wrong well while the following pulse occurs, or on the contrary, the thermal noise could counter the

effect of the current pulse and the DW could stay pinned in the nondesired potential well.

To carry out this study, we computed the DW dynamics at $T = 293$ K for finite/infinite nanostrip and different pulse shapes. The results are shown in Fig. 4. In all cases, panels (a) to (d), the DW first oscillates freely (relaxation) in the presence of the thermal noise in its initial well during 10 ns and afterwards a current pulse is applied to push the DW to another well (corresponding to one of the bands in Figs. 2 and 3), followed by a DW relaxation during another 10 ns. The damping parameter α is taken as 0.02, lower than the one at $T = 0$ K [38], and the nonadiabatic parameter is taken as $\beta = 2\alpha = 0.04$. The same phase diagrams, as presented in Figs. 2 and 3, were recalculated with $\alpha = 0.02$ and $\beta = 0.04$ at $T = 0$ K and these bands, from one to four, are indicated by dotted lines in Fig. 4(a) for the finite nanostrip, while the bands from one to seven are indicated in panels (b) to (d) for the infinite nanostrip. Starting from the fourth band, the shape of the bands changes showing a reentrant transition [except panel (c)], and the phase diagrams from panels (b) to (d) show band pockets to the left corresponding to negative DW displacement of one notch (noted as band -1) even though the STT pushes the DW in the positive direction. These features are discussed in Sec. III C.

The stochastic motion of the DW was computed for a number of bands with the stochastic 1D model, and only on a certain number of points micromagnetically. Figure 4(a)

shows the probability of the DW motion in the first four bands for a finite nanowire, when a symmetric current pulse ($t_r = t_f = 5$ ps) is applied after a relaxation time of 10 ns. At the end of the pulse, the DW is relaxed another 10 ns before its position is considered acquired. A certain number of realizations was computed for a quarter of the phase diagram points of each band: 2700 realizations for each point shown from the first band and 500 realizations for each point of the superior bands. The maximum of probability (100%) for the precise positioning of the DW to the nearest notch is found only for 0.76% of the first band's calculated points (17 points), while on 32.18% of the points the probability is superior to 95%. The maximum of probability decreases rapidly with increasing the band number, being 98.6% (for three points) for the second band, 67.4% for the third band, and 71% for the fourth band. These results are to be compared with panel (b), where the same pulse is applied in an infinite nanowire and the same number of realizations were computed for each band. The maximum probabilities are similar for the first two bands, for similar band point number density, indicating that at room temperature only few current pulse characteristics give 100% probability of precise positioning. The points in the first band, that correspond to 100% probability of desired motion, appear for an applied current superior to 7.7 A/μm^2 and a pulse length between 100 ps and 130 ps for the finite strip and superior to 8.1 A/μm^2 and a pulse length between 90 ps and 120 ps for the infinite case, respectively. For superior bands, starting with the fourth, the maximum of probability and band point number density are increased in the infinite nanostrip compared to the finite case, as in the latter the potential barrier is weaker for the more distant notches [see Fig. 1(c)]. Micromagnetically, we computed the probability for the phase diagram points corresponding to the 100% values found with the 1D model (which appear only in the first band) on 200 realizations/point. These probabilities vary between 92% and 97%. The small difference between the probability calculations of the micromagnetic and 1D model is attributed to the small shift in the phase diagrams that was shown to exist between the two.

Figures 4(c) and 4(d) show the probability of DW motion when an asymmetric current pulse is applied after 10 ns initial and final relaxation. The pulse shape is $t_r = 5$ ps, $t_f = 300$ ps in panel (c) and $t_r = 300$ ps, $t_f = 5$ ps in panel (d). The maximum of probability in the first band of panel (c) is 96.77%, with only 2.31% of calculated band points having a probability superior to 95% (from 2700 realizations). For the superior bands, the maximum of probability diminishes with only 2.93% of points having a probability superior to 90% in the second band and 2.32% of points having a probability superior to 80% in the third band. For panel (d), the maximum of probability in the first band is found to be 98.07%, with 7.69% of points having a probability superior to 95%. The maximum of probability diminishes faster in the superior bands as compared with the panel (c) results, with less points having maximum band probability. For example, only 0.79% of points have a probability superior to 90% in the second band and 0.54% of points have a probability superior to 80% in the third band. The difference in probability between the two asymmetric pulses is due to the fact that the long rise time of the pulse [panel (d)] produces the shift up and right of the bands compared with panel (c); therefore, more points

with maximum probability are found in the first band (as these points are usually close to the band center) and lower points with maximum probability in the superior bands as there are less points on these bands.

These results suggest that to achieve a well defined DW positioning at room temperature by STT alone, individual pulses should be applied with very short rise and fall time.

C. Influence of α and β on the DW dynamics

The influence of the damping parameter α and of the nonadiabatic parameter β on the phase diagram for an infinite strip at $T = 0$ K is detailed in Fig. 5. The damping parameter α was varied between 0.02 and 0.05, which correspond to the zero and room temperature values [38]. The nonadiabatic parameter was varied between zero and 2α. The case with $\beta = 2\alpha$ is shown in Fig. 2(b) and Fig. 4(b) for $\alpha = 0.05$ and 0.02, respectively. The computations with $\beta = 0$ are presented in panels (a) and (b) of Fig. 5, while the ones with $\beta = \alpha$ are displayed in panels (c) and (d). We observe that for $\alpha = 0.05$, when β is diminished from 2α to zero, important changes appear in the phase diagram only when β is less than α. In this case [panel (a)], the results obtained with the 1D model (colored regions) exhibit only the first band (band +1) with large pockets of negative numbered bands. In all cases, the DW is pushed initially by the current pulse in the positive direction (to the right), so a negative band expresses a DW position at the end of the pulse to the left of the initial notch, in the opposite direction of the STT. The micromagnetic computations confirm this behavior, which was predicted and observed before [13,20,21,27]. Due to the pinning potential, the DW deforms and can change its internal structure giving rise to a transient motion associated with DW inertia. The transient DW movement is proportional to the variation of the generalized angle of the wall:

$$\delta X = -\frac{\Delta}{\alpha}\left(1 - \frac{\beta}{\alpha}\right)\delta\psi, \tag{4}$$

with ψ the azimuthal angle of the wall. For $\beta = 0$, the transient motion is increased for large DW width or small damping parameter. This effect is displayed in Fig. 5(b) for $\alpha = 0.02$, as compared with panel (a), where an increased number of negative bands are visible. For the ultrashort current pulses used, which are comparable with the DW damping time τ_d, the transient effects dominate at low damping parameter.

A discrepancy is found between the micromagnetic results (symbols) and the 1D results in the upper right quadrant (high current, longer pulse) for the phase diagrams with $\beta = 0$. This discrepancy is due to the large angle variation at large current and longer pulse that leads to the transformation of the transverse DW and the creation of an antivortex close to the initial notches before depinning [39] (see figure and movie in the Supplemental Material [36]). DW velocity boosting was predicted through antivortex generation at a singular notch in a nanostrip [40]. The antivortex disappear quickly after the end of the current pulse, and in certain cases can reverse the orientation of the magnetization at the center of the transverse DW leading to DW motion in the opposite direction. The antivortex does not appear in all the computed micromagnetic
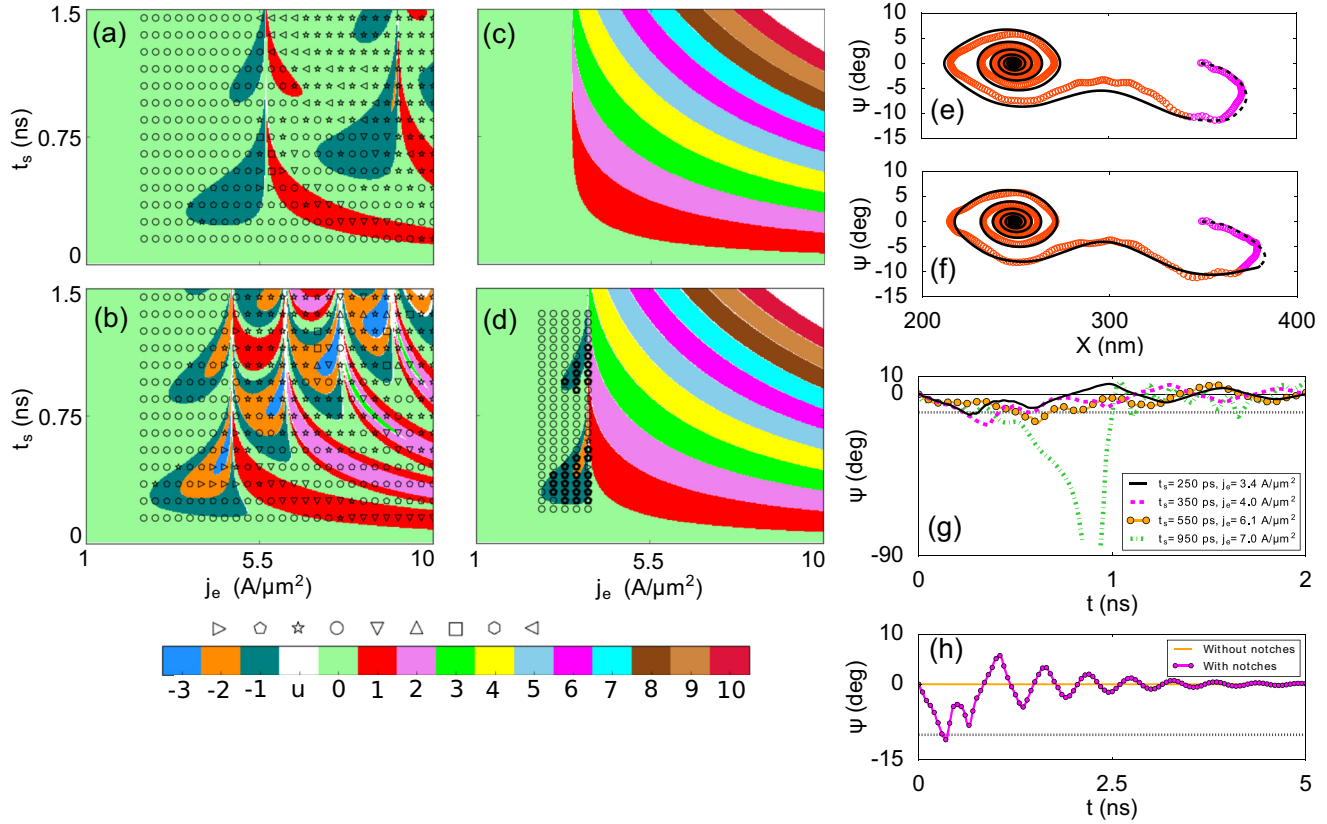
FIG. 5. Influence of the damping parameter α and nonadiabatic parameter β on the phase diagram for an infinite strip at $T = 0$ K: (a) $\alpha = 0.05$ and $\beta = 0$, (b) $\alpha = 0.02$ and $\beta = 0$, (c) $\alpha = \beta = 0.05$, and (d) $\alpha = \beta = 0.02$. A sequence of symmetric pulses with the same characteristics as in Fig. 2 are applied. The scattered symbols represent the micromagnetic results, while the colored regions are calculations with the 1D model. Trajectories in the phase space (X, ψ) corresponding to the -1 band in panels (b) [(d)]: (e) $t_s = 250$ ps, $j_e = 3.4$ A/μm^2, $\alpha = 0.02$, $\beta = 0$ and (f) $t_s = 300$ ps, $j_e = 3.6$ A/μm^2, $\alpha = \beta = 0.02$. The scattered symbols and the full line represent the micromagnetic and the 1D results, respectively. The dotted part of the full line indicates the applied pulse duration. (g) DW angle variation for $\alpha = 0.02$, $\beta = 0$ for several points in the panel (b). (h) Comparison of the DW angular variation for $\alpha = \beta = 0.02$ and $t_s = 300$ ps, $j_e = 3.6$ A/μm^2 for the infinite strip with notches [band -1 in panel (d)] and strip without notches.

results in the upper right quadrant of these phase diagrams. In the 1D model, the antivortex nucleation is not taken into account.

As is obvious from Eq. (4), for $\beta = \alpha$ the transient motion is somehow blocked and the DW travels rigidly. This seems to be the case for $\beta = \alpha = 0.05$, as computed in the phase diagram shown in Fig. 5(c). However, when $\beta = \alpha = 0.02$, the negative bands are still present at low currents [panel (d)] without the apparition of an antivortex. This effect was verified micromagnetically on a number of points (empty symbols), which compare very well with the 1D results. The pocket form of the -1 band is respected with a small shift, even a -2 band was observed micromagnetically corresponding to the small -2 pocket inside the -1 band. The DW motion in the case $\beta = \alpha$ can be well explained analyzing the 1D equations of motion of the DW:

$$(1 + \alpha^2)\dot{X} = -\frac{\alpha\gamma\Delta}{2\mu_0 M_s S}\frac{\partial E}{\partial X} + \frac{\gamma\Delta}{2}H_k \sin 2\psi + (1 + \alpha\beta)u,$$

$$(1 + \alpha^2)\dot{\psi} = -\frac{\gamma}{2\mu_0 M_s S}\frac{\partial E}{\partial X} - \frac{\gamma\alpha}{2}H_k \sin 2\psi + \frac{\beta - \alpha}{\Delta}u,$$

$$(5)$$

where S is the section of the wire, γ the gyromagnetic ratio, and H_k the DW demagnetizing field. E is the pinning potential energy which is assumed parabolic inside the notch. The DW width variation is given by $\Delta(t) = \Delta[\Psi(t)] = \pi\sqrt{\frac{2A}{\mu_0 M_S^2 \sin^2 \psi + \mu_0 M_S H_k}}$. From the above equations, one can notice that the azimuthal DW angle ψ and DW position X depend on the pinning potential (restoring force) created by the symmetric notches. When a current pulse is applied, the DW is first compressed and distorts on the potential barrier moving in the direction of the STT, while the azimuthal angle decreases in some cases below $-10°$ (dotted line), as is displayed in Fig. 5(h) (videos and additional figures in the Supplemental Material [36]). Initially, the STT pushes the DW in the positive direction, resulting in a positive DW velocity and a negative restoring force (negative DW angle). If the DW does not have enough velocity to surpass the potential barrier in this direction, it goes down the potential well towards the center of the notch and the restoring force still stays negative, while the velocity and angle continue to decrease with the velocity becoming negative. When the DW starts to mount the potential well in the other direction, the restoring force becomes positive so the velocity and DW angle

start to increase [Fig. 5(f)]. When the current pulse ends, the velocity decreases abruptly (increases in absolute value) and ψ increases lightly due to the short fall time. At this moment, the DW position inside the potential well is important as it imposes a restoring force in the direction of movement or in the opposite direction. However, the velocity and the DW angle are equally important for the jump to the previous notches to happen (see Supplemental Material [36]). The jump occurs therefore due to a combination of factors, even if the restoring force is positive or negative. The presence of the notch pinning potential induces the DW distortion and therefore the transient motion, as for the same pulse parameters no observable angle variation is determined for a perfect strip. As the variation of the DW angle is directly related to the variation in position, the automotion is possible in this case triggered by the pinning induced DW distortion, restoring potential force and smallness of the damping parameter.

In Fig. 5(g), several angular variations are presented corresponding to the -1 and -2 bands from panel (b). We observe that the amplitude of angular variation is directly proportional with the spatial displacement. When an antivortex appears, the DW angle rotates out of plane and the DW position does not correspond anymore to the 1D results and the motion opposite to the STT can be completely blocked. In general, we observe the automotion in all the cases when the DW angle increases above $10°$ (in absolute values) during or after the current pulse and the maximum DW velocity is close or superior to 400 m/s (details in the Supplemental Material [36]). Exactly at the boundary between the -1 band and the zero band (pinned state), a small increase in the azimuthal angle of $0.2°$ and of the DW velocity by 5 m/s at the end of the current pulse, between two points in different bands, is enough to promote a DW jump to a previous notch.

The transient effects also appear when $\beta > \alpha$, as depicted in Fig. 4 for $\beta = 2\alpha = 0.04$. A low value of the damping parameter α is required to obtain observable consequences. A particularity of the case $\beta > \alpha$ is that the transient effects oppose or amplify the STT, as negative bands are determined and a reentrant transition is seen at higher currents and pulse length in panels (b) and (d). The transient effects depend on the pulse shape (see Supplemental Material [36]), as for the asymmetric pulse with $t_r = 5$ ps, $t_f = 300$ ps, the band -1 is barely visible and no reentrant transition of the bands is seen, while the -1 band increases when the pulse is symmetric and continues to increase, with even a second -1 band appearing at larger t_s for the asymmetric pulse with $t_r = 300$ ps, $t_f = 5$ ps. The fall time t_f plays an important role in the value of the DW velocity and DW angle at the end of the current pulse, as a short t_f leads to a very high DW velocity and a higher DW angle at the end of the pulse increasing the impact of transient effects and inducing a DW depinning. Contrary to earlier beliefs [13], the DW depinning does not necessarily result from a large DW angle or the DW position at the end of the pulse. A maximum DW angle and DW velocity large enough during the current pulse suffice to ensure for example the jump to the previous notch, even if the angle is not that large (and at its maximum) at the pulse end, as observed in the case of the asymmetric pulse with $t_r = 5$ ps, $t_f = 300$ ps (see Supplemental Material [36]). This is purely a transient effect due to a combined action of the pinning potential, low α and pulse shape.
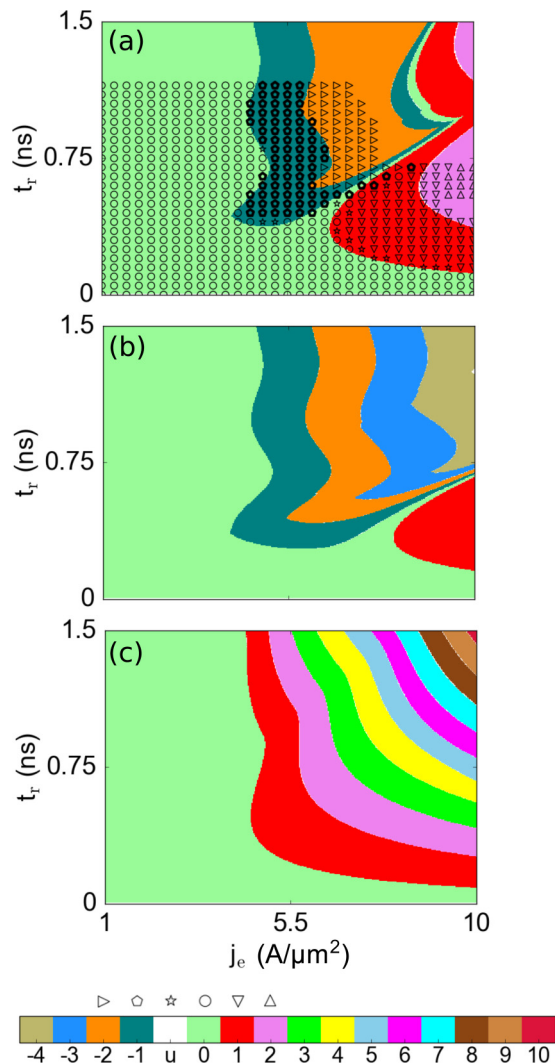

FIG. 6. Influence of the pulse raise time t_r on the phase diagram for a DW at $T = 0$ K in an infinite nanostrip for different parameters α and β. The parameter space is the raise time vs current amplitude. In all cases, $t_s = t_f = 5$ ps and $t_z = 10$ ns. (a) $\alpha = 0.02$ and $\beta = 0.04$, (b) $\alpha = \beta = 0.02$, and (c) $\alpha = 0.05$ and $\beta = 0.1$. In (a) the micromagnetic results (scattered symbols) are compared to the 1D model (colored regions), while in (b) and (c) only 1D model results are shown. At high currents, the micromagnetic results give several unintended states [the empty scattered symbol region to the right of (a)].

The influence of the rise time t_r on the phase diagrams is presented in Fig. 6 for $t_s = t_f = 5$ ps and several parameters α and β. The rise time is varied between 0 and 1.5 ns (case of a very asymmetric pulse). A first observation is that the first depinning current is increased as the force term that depends on the current derivative in Eq. (3) diminishes. The first depinning current actually oscillates with t_r due to resonant effects, as the resonant frequency of the potential well is around 1.75 GHz. This resonant effect is more important for the bands with negative numbers for low α, as is depicted in panels (a) and (b) for $\alpha = 0.02$ and $\beta = 0.4$ or 0.2, respectively. The 1D model gives good quantitative results as compared with the micromagnetic calculations, as shown in panel (a), although a

small shift is again found at high currents and more unwanted states. When $\beta \leqslant \alpha$, the positive bands are shifted to very high current, with only negative bands remaining for $\beta = 0$ (image not shown). The phase diagram for $\alpha = 0.05$ and $\beta = 0.1$, also shown in panel (c), still does not present negative bands but the same oscillation of the first depinning current and of the interband transitions.

The influence on the phase diagram is less dramatic when varying the fall time t_f (images shown in the Supplemental Material [36]). For $\alpha = 0.02$ and $\beta > \alpha$ no negative bands appear and the positive bands are shifted to larger currents. When $\beta \leqslant \alpha = 0.02$, only a small pocket of the -1 band appears and the positive bands are shifted as compared with Fig. 5(d).

IV. DISCUSSION AND CONCLUSION

The presence of artificial constrictions in a nanostrip influences drastically the movement of a magnetic DW. When ultrashort current pulses are applied, the DW can exhibit an important distortion at the notch depending on the pulse characteristics. Thereby, the DW displays inertialike effects, which can have dramatic consequences on its transient displacement. These effects depend largely on the damping parameter α and on the nonadiabatic parameter β. For $\beta < \alpha$, these effects generally oppose the STT effect after the pulse end and DW motion in the direction of the electric current is possible. If $\beta > \alpha$, these effects oppose or amplify the STT effect and jumps to the left or the right notches are possible after the end of the pulse. The transient effects in this case depend on the pulse characteristics. This could constitute another way of experimentally comparing the two parameters α and β for a ferromagnetic material.

At room temperature, the jump probability to the desired notches decreases with increasing band number, each band number corresponding to a positioning to desired notches in the direction of the STT. Maximum positioning probability is reached only for very short rise and fall time to the nearest neighbors notches only. Therefore, to shift reliably the DWs between notches, current pulses corresponding to displacement from one symmetric notch to the closest neighbors should be used. The shape of the current pulse influences the depinning current and shifts the bands. The phase diagram for the case of two domain walls situated at different symmetric notches (images not shown), that are displaced by the same current pulse in the same direction, is very similar with the ones presented in Sec. III, but the bands are narrower and the interband depinning is larger between the first bands.

The main drawback of the classical DW displacement under STT alone compared with more exotic torques (of spin-orbit origin) is the high current values necessary. The current induces Joule heating in the nanostrip that can largely increase the temperature and could even destroy the ferromagnetic state. The increase in temperature is even more important at the constrictions in the nanostrip. Several theoretical studies were dedicated to Joule heating in nanowires [41–44], usually considering a standard Py nanostrip on a Si/SiO_2 substrate. We evaluated the temperature increase for our Ni strips on different substrates like pure Si, SiO_2, or Ni_3Si_4 membranes for a current pulse length of 1 ns. On pure Si, considering an infinite 3D substrate [41], the temperature increase is negligible being of 4 K for $j = 5$ A/μm^2 (17 K for $j = 10$ A/μm^2). However, on SiO_2 substrate of 300 nm thickness [42], the temperature increase is larger, being 26 K for $j = 5$ A/μm^2 (103 K for $j = 10$ A/μm^2). If 100 nm thick Ni_3Si_4 membranes are used [15,42], the temperature increase is of 41 K for $j = 5$ A/μm^2 (163 K for $j = 10$ A/μm^2). The variation in temperature depends on the material parameters of the substrate (like thermal conductivity) and on the conductivity of the nanostrip. In the above estimations, the bulk Ni room temperature conductivity was used ($\sigma^{-1} = 7.3\ \mu\Omega$ cm) [45]. If the dimensions are reduced to nanometers [46], the conductivity of Ni can vary drastically (a factor four) and the temperature increase can be more important, but in the main time the length of the current pulse that amounts to the maximum probability at room temperature is around 0.1 ns, which reduces significantly the temperature increase.

In conclusion, systematic DW motion between precise artificial pinning constriction by very short current pulses is possible at room temperature in a classical ferromagnet. The constrictions induce DW distortions and important transient effects can be observed. Depending on the ratio β/α, the inertialike effect can oppose or amplify the STT effect on the DW motion after the pulse end. As the value of β is still under debate, this could constitute another way of determining its relative value. Our results open the path to DW motion in both directions by unipolar current pulses.

ACKNOWLEDGMENTS

[1] L. Thomas and S. S. P. Parkin, *Handbook of Magnetism and Advanced Magnetic Materials* (Wiley, New York, 2007).

[2] O. Boulle, G. Malinowski, and M. Kläui, Mater. Sci. Eng. R **72**, 159 (2011).

[3] S. S. P. Parkin, M. Hayashi, and L. Thomas, Science **320**, 190 (2008).

[4] D. A. Allwood, G. Xiong, C. C. Faulkner, D. Atkinson, D. Petit, and R. P. Cowburn, Science **309**, 1688 (2005).

[5] D. Petit, A.-V. Jausovec, D. Read, and R. P. Cowburn, J. Appl. Phys. **103**, 114307 (2008).

[6] D. Petit, A.-V. Jausovec, H. T. Zeng, E. Lewis, L. O'Brien, D. Read, and R. P. Cowburn, Phys. Rev. B **79**, 214405 (2009).

[7] E. Martinez, L. Lopez-Diaz, O. Alejos, L. Torres, and M. Carpentieri, Phys. Rev. B **79**, 094430 (2009).

[8] V. O. Dolocan, Appl. Phys. Lett. **105**, 162401 (2014).

[9] A. Pivano and V. O. Dolocan, J. Magn. Magn. Mater. **393**, 334 (2015).

[10] V. O. Dolocan, Eur. Phys. J. B **87**, 188 (2014).

[11] A. Pivano and V. O. Dolocan, Phys. Rev. B **93**, 144410 (2016).

[12] E. Martinez, G. Finocchio, and M. Carpentieri, Appl. Phys. Lett. **98**, 072507 (2011).

[13] L. Thomas, M. Hayashi, X. Jiang, R. Moriya, C. Rettner, and S. S. P. Parkin, Nature (London) **443**, 197 (2006).

[14] L. Thomas, M. Hayashi, X. Jiang, R. Moriya, C. Rettner, and S. S. P. Parkin, Science **315**, 1553 (2007).

[15] L. Bocklage, B. Krüger, T. Matsuyama, M. Bolte, U. Merkt, D. Pfannkuche, and G. Meier, Phys. Rev. Lett. **103**, 197204 (2009).

[16] P. Yan and X. R. Wang, Appl. Phys. Lett. **96**, 162506 (2010).

[17] H. H. Langner, L. Bocklage, B. Krüger, T. Matsuyama, and G. Meier, Appl. Phys. Lett. **97**, 242503 (2010).

[18] B. Krüger, D. Pfannkuche, M. Bolte, G. Meier, and U. Merkt, Phys. Rev. B **75**, 054421 (2007).

[19] L. Heyne, J. Rhensius, A. Bisig, S. Krzyk, P. Punke, M. Kläui, L. J. Heyderman, L. Le Guyader, and F. Nolting, Appl. Phys. Lett. **96**, 032504 (2010).

[20] A. Thiaville, Y. Nakatani, F. Piechon, J. Miltat, and T. Ono, Eur. Phys. J. B **60**, 15 (2007).

[21] J. Y. Chauleau, R. Weil, A. Thiaville, and J. Miltat, Phys. Rev. B **82**, 214414 (2010).

[22] L. Thomas, R. Moriya, C. Rettner, and S. S. P. Parkin, Science **330**, 1810 (2010).

[23] J. Rhensius, L. Heyne, D. Backes, S. Krzyk, L. J. Heyderman, L. Joly, F. Nolting, and M. Kläui, Phys. Rev. Lett. **104**, 067201 (2010).

[24] T. Taniguchi, K.-J. Kim, T. Tono, T. Moriyama, Y. Nakatani, and T. Ono, Appl. Phys. Exp. **8**, 073008 (2015).

[25] X. R. Wang, P. Yan, J. Lu, and C. He, Ann. Phys. (NY) **324**, 1815 (2009).

[26] M. Yan, A. Kakay, S. Gliga, and R. Hertel, Phys. Rev. Lett. **104**, 057201 (2010).

[27] J. Vogel, M. Bonfim, N. Rougemaille, O. Boulle, I. M. Miron, S. Auffret, B. Rodmacq, G. Gaudin, J. C. Cezar, F. Sirotti, and S. Pizzini, Phys. Rev. Lett. **108**, 247202 (2012).

[28] T. Janda, P. E. Roy, R. M. Otxoa, Z. Soban, A. Ramsay, A. C. Irvine, F. Trojanek, M. Surynek, R. P. Campion, B. L. Gallagher, P. Nemec, T. Jungwirth, and J. Wunderlich, Nat. Commun. **8**, 15226 (2017).

[29] J. Torrejon, E. Martinez, and M. Hayashi, Nat. Commun. **7**, 13533 (2016).

[30] H. Y. Yuan and X. R. Wang, Phys. Rev. B **89**, 054423 (2014).

[31] A. Vansteenkiste, J. Leliaert, M. Dvornik, M. Helsen, F. Garcia-Sanchez, and B. Van Waeyenberge, AIP Adv. **4**, 107133 (2014).

[32] J. C. Slonczewski, J. Appl. Phys. **45**, 2705 (1974).

[33] A. Thiaville and Y. Nakatani, in *Spin Dynamics in Confined Magnetic Structures III*, edited by B. Hillebrands and A. Thiaville (Springer, Berlin, 2006).

[34] S. Zhang and Z. Li, Phys. Rev. Lett. **93**, 127204 (2004).

[35] M. E. Lucassen, H. J. van Driel, C. M. Smith, and R. A. Duine, Phys. Rev. B **79**, 224411 (2009).

[36] See Supplemental Material at http://link.aps.org/supplemental/10.1103/PhysRevB.96.224431 for details of parameters influence on phase diagram.

[37] B. Krüger, J. Phys.: Condens. Matter **24**, 024209 (2012).

[38] K. Gilmore, Y. U. Idzerda, and M. D. Stiles, Phys. Rev. Lett. **99**, 027204 (2007).

[39] H. Y. Yuan and X. R. Wang, Eur. Phys. J. B **88**, 214 (2015).

[40] H. Y. Yuan and X. R. Wang, Phys. Rev. B **92**, 054419 (2015).

[41] C. Y. You, I. M. Sung, and B. K. Joe, Appl. Phys. Lett. **89**, 222513 (2006).

[42] H. Fangohr, D. S. Chernyshenko, M. Franchin, T. Fischbacher, and G. Meier, Phys. Rev. B **84**, 054437 (2011).

[43] S. Moretti, V. Raposo, and E. Martinez, J. Appl. Phys. **119**, 213902 (2016).

[44] S. Lepadatu, J. Appl. Phys. **120**, 163908 (2016).

[45] G. K. White and S. B. Woods, Philos. Trans. R. Soc. London A **251**, 273 (1959).

[46] M. N. Ou, T. J. Yang, S. R. Harutyunyan, Y. Y. Chen, C. D. Chen, and S. J. Lai, Appl. Phys. Lett. **92**, 063101 (2008).